Predictive Current Control for Stabilizing Power Electronics Based AC Power Systems

M A Awal, Iqbal Husain, Wensong Yu
FREEDM Systems Center
North Carolina State University
Raleigh, USA
Email: mawal@ncsu.edu

***Abstract*— Frequency domain passivity theory is used to evaluate harmonic resonance instabilities in a system with multiple grid-tied voltage source converters (VSCs), and subsequently, a stabilizing controller using predictive current control (PCC) method is proposed to prevent such instabilities. The input admittance of VSCs using PCC can achieve passivity almost up to the Nyquist frequency. This research demonstrates that a very simple and easy implementation of PCC can extend the controller delay dependent stability range of converter side current control for VSCs equipped with LCL-filters up to that point. The alternative approaches achieved stability over similar frequency range by combining complicated active damping techniques with proportional-integral or proportional-resonant type controllers. The frequency domain analysis of the proposed PCC based method is validated via simulation and hardware experiments. The controller is experimentally shown to achieve stable operation irrespective of model imperfections.**

Keywords—Predictive current control; passivity; admittance; harmonic resonance, stability

I. INTRODUCTION

Power electronic converters as power processing and interfacing units have been penetrating into numerous grid applications, such as distributed generation, flexible ac transmission systems, microgrids, and high voltage dc (HVDC) transmission systems due to their superior harmonic performance, efficiency, and controllability. However, as these units are actively controlled, they introduce highly nonlinear and time varying dynamics and the interaction among different units may lead to instability in interconnected systems. The stability issues of current controlled grid-tied VSCs equipped with LCL filters in case of grid impedance variation is well-studied and a number of passive [1] and active damping or virtual resistor based methods [2-3] have been proposed. However, passive damping techniques incur loss and all these resonance damping techniques fail beyond a critical frequency depending on the controller delay time. Stability issues of grid-tied parallel inverters have been studied and controller design guidelines based on the so called 'Minor Loop Gain (MLG)' or 'Global Minor Loop Gain (GMLG)' have been proposed for a range of grid impedance values [4]. For such converters which interact through grid impedance, hardware-active-dampers have also been proposed which are similar to active power filters [5]. This type of instability occurs when the interconnected network has poles in a frequency range where the converter input admittance is not passive. A passive input admittance, i.e., non-negative real part up to Nyquist frequency, is quite difficult to achieve due to the controller delay. Methods have been proposed to eliminate computational delay completely, but to achieve that control calculations have to be completed in a quarter of a switching period which becomes quite challenging for low cost applications with relatively less powerful microcontrollers [6]. It is well known that without the elimination of controller delay, for converter side current control of VSCs equipped with LCL-filters, one has to employ active damping to stabilize harmonic resonances above a critical frequency set by the delay [7]. Frequency domain passivity based active damping has shown to achieve stability irrespective of grid impedance variation as long as the system resonant points are located below the Nyquist point [8-10]. A sensor less passivity based damping injection method has also been proposed, but it requires significant numerical analysis to maximize the stable frequency range [7]. All the available methods either require additional sensors or involve complicated implementation. To the contrary, predictive control is very simple and easy to implement compared to the aforementioned methods. Even though it has been studied for grid-tied applications previously [11,12], but to the best of the authors' knowledge, the passive admittance, and hence, the stabilizing property of predictive controllers irrespective of any variation in grid impedance and other interconnected units has not been investigated. In this work, the input admittance for the predictive current control (PCC) is derived using a continuous-time model. Using frequency domain passivity theory based analysis, it is shown that the PCC can stabilize harmonic resonances almost up to the Nyquist point. Sensitivity of PCC to model imperfections is also investigated experimentally and the performance was found to be satisfactory.

The rest of the paper is organized as follows. At first a system of multiple grid tied VSCs is described and the impedance model of such a VSC is developed. Then a frequency domain passivity based stability criterion is specified for a VSC while interacting with the rest of the system, and two different cases of harmonic resonance instability are demonstrated. Then a PCC method is proposed to stabilize these interactions. Using Laplace domain analysis, an input admittance model for PCC is derived. The admittance has been found to be passive almost up to the Nyquist point, and hence, can prevent harmonic resonance instability up to that frequency. Finally, it is experimentally demonstrated that the controller performs satisfactorily irrespective of model imperfections.

II. System Description

Fig. 1 shows a system of multiple grid-tied VSCs equipped with LCL filters. The results from the frequency domain analysis in the following sections are applicable for single phase systems or per-phase control of three phase systems in the stationary reference frame. For stationary $\alpha\beta$-frame controller implementation, variables are to be assumed as space vectors. The converter side inductors, grid side inductors and capacitors of the LCL input filters are denoted as L_{1_n}, L_{2_n} and C_n, respectively for $n = 1,2 \ldots N$. Here, Z_{g_n} for $n = 2 \ldots N$ represent the line impedances whereas Z_{g_1} also includes the grid impedance. It is to be noted that all parasitic resistances in converter reactive components as well as transmission line resistances are ignored to consider the worst-case scenario in terms of stability. The DC link voltage is denoted as V_{dc_n} whereas the voltage averaged over one switching period T_s, established across the poles by the switch network is taken as v_{m_n} which can be expressed as the product of switching duty ratio and the DC link voltage. The current through the converter side and grid side inductors are denoted as i_{L_n} and i_{g_n}, respectively, and v_{c_n} is the voltage across filter capacitor C_n.

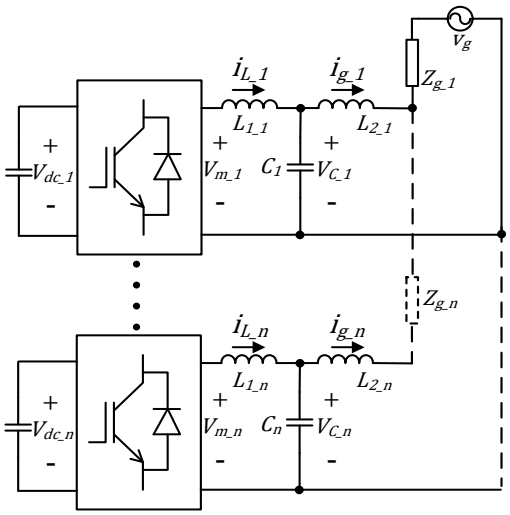

Fig. 1. System of multiple grid-tied VSCs.

III. Impedance Model

The dynamics of the converter side inductor current is given by

$$L_{1\_n}\frac{di_{L\_n}}{dt} = v_{m\_n} - v_{c\_n} \tag{1}$$

The effective voltage across the inductor is contributed by both the converter voltage v_{m_n} and the capacitor voltage v_{c_n}. The capacitor voltage is directly affected by the grid voltage. Fig. 2 shows one possible choice for converter side current control where $F_c(s)$ denotes a linear controller which can be of proportional-integral (PI) or proportional-resonant (PR) type and the capacitor voltage is used as a feedforward signal through a filter $H_F(s)$. Instead of capacitor voltage feedforward, active damping techniques can also be employed. For digital implementation, the controller includes one-sample calculation

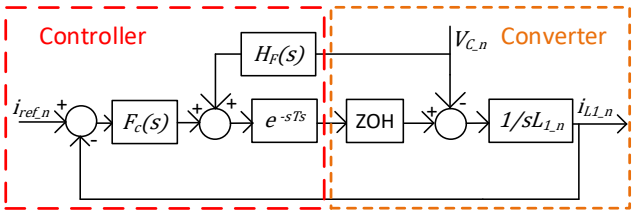

Fig. 2. Equivalent model of power stage with linear controller and voltage feedforward.

delay. The power stage is modelled with unity gain. With this choice of controller, the converter side inductor current is given as

$$i_{L\_n}(s) = T_n(s) \times i_{ref\_n} - Y_n(s) \times v_{c\_n}(s) \tag{2}$$

where

$$T_n(s) = \frac{e^{-sT_S}F_{zoh}(s)F_c(s)}{sL_{1\_n}+e^{-sT_S}F_{zoh}(s)F_c(s)} \tag{3}$$

$$Y_n(s) = \frac{1-e^{-sT_S}F_{zoh}(s)H_F(s)}{sL_{1\_n}+e^{-sT_S}F_{zoh}(s)F_c(s)} \tag{4}$$

$$F_{zoh}(s) = \frac{1-e^{-sT_S}}{sT_S} \tag{5}$$

Here $T_n(s)$ is the reference to output response and $Y_n(s)$ is the input admittance. Using (2), the n-th VSC can be modelled as in Fig. 3 where $Z_{eq\_n}(s)$ denotes the equivalent impedance seen by the VSC which includes the capacitor and grid side inductor of its own input filter, line impedances, and the rest of the system.

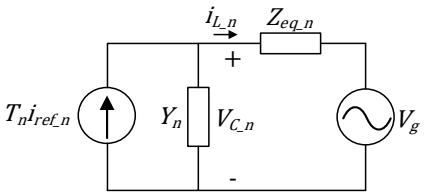

Fig. 3. Admittance model of converter side current controlled VSC.

$$V_{C\_n}(s) = i_{L\_n}(s)Z_{eq\_n}(s) + V_g(s) \tag{6}$$

Substituting (6) into (2) gives

$$i_{L\_n}(s) = \frac{T_n(s)}{1+Y_n(s)Z_{eq\_n}(s)} \times i_{ref\_n} - \frac{Y_n(s)}{1+Y_n(s)Z_{eq\_n}(s)} \times V_g(s) \tag{7}$$

The stability of the equivalent system is defined by the poles of $1 + Y_n(s)Z_{eq\_n}(s) = 0$. It is to be noted that the VSC admittance and the equivalent impedance seen by the VSC looking into the grid at the interfacing point form a minor feedback loop, which determines the system stability [7, 13].

IV. Frequency Domain Passivity Based Stability Analysis

$F_c(s)$ is designed to give a stable closed loop response $T_n(s)$ which makes the VSC current control loop internally stable.

However, $Y_n(s)$ interacts with the grid impedance through a minor feedback loop. With infinite resolution sampling, i.e. $H_F(s) = 1$, and instantaneous control, i.e., total delay $T_d = 0$, the effect of input admittance could be negated giving $Y_n(s) = 0$, which makes the current control loop externally stable for any grid condition. But for practical systems there is a finite time delay and in most applications $T_d = 1.5T_s$ of which one switching period is due to calculations and other half period delay is contributed by PWM which is a reasonable approximation for most modulation techniques [14]. It is to be noted that a ZOH gives the same phase response as $0.5T_s$ delay.

Frequency domain passivity theory has been used to assess the stability of the minor feedback loop formed by $Y_n(s)$ and $Z_{eq\_n}(s)$ [7, 10]. The input admittance $Y_n(s)$ is said to be passive in the frequency range of interest if it can be shown that it is stable and has non-negative real part in that particular frequency range. If both $Y_n(s)$ and $Z_{eq\_n}(s)$ are passive in a specific frequency range, then according to frequency domain passivity theory, their feedback interaction is stable over that range. Both $Y(s)$ and $Z_{eq}(s)$ to be passive is a sufficient condition, but not a necessary one as it will be shown in later sections. Another intuitive interpretation of passivity is that non-negative real part of admittance corresponds to resistive behavior leading to consumption of energy or damping. A negative conductance behavior over a range of frequencies signifies amplification of disturbance or oscillation at any frequency within that range.

Identifying the frequency range of interest is an important step in the design and analysis process. Continuous-time representations, i.e. in Laplace domain, do not model the aliasing effects introduced by the sampling of the states by the controller. Therefore, such analysis is not suitable at frequencies beyond the Nyquist point, i.e. $f_s/2$. A recent work reported design considerations for LCL filters with resonant frequencies beyond the Nyquist point where the power stage is approximated with a simple ZOH and the analysis is done in the discrete-time domain [15]. Theoretically, at higher frequencies such as close to Nyquist point, a model loses accuracy significantly with a ZOH approximation. Another approach may be a multiple-frequency admittance model where the controller is transformed into continuous time domain instead [16]. However, none of these methods consider the intermodulation products present in the PWM spectrum. For uniform sampling of the modulating wave, a symmetrical double-edge PWM spectrum gives a non-linear function of the modulating wave within the baseband, i.e. below the Nyquist frequency [17]. It is exceedingly difficult to derive an accurate model of a sampled data system in the frequency domain beyond the Nyquist point, and as such, the benefits of the aforementioned complicated analysis methods are to be weighed against the attainable accuracy that they offer. Therefore, further analysis in this paper is shown up to the Nyquist point. It has been in prior research shown that the negative conductance region of converter side current control for a single update mode PWM implementation starts at $f_{crit} = 1/4T_d$ [7]. This non-passive input admittance may give rise to harmonic resonance. Two such scenarios are demonstrated in the following subsections. In *Case 1*, a small grid impedance is shown to destabilize the current control loop for a single grid-tied VSC; and in *Case 2*, addition of an identical VSC is shown to destabilize a stable pre-existing converter.

A. Case 1: Single VSC and grid impedance interaction

Table I shows the filter and controller parameters for a single-phase grid-tied VSC. Proportional resonant controller is implemented in the stationary frame and has the following form.

$$F_c(s) = K_P + \sum_h K_{R,h} \times \frac{s}{s^2 + (h\omega_1)^2} \quad (8)$$

Here, K_P is the proportional gain and $K_{R,h}$ is the resonant gain at h-th harmonic of the fundamental frequency ω_1 rad/s. No feedforward is used, i.e., $H_F(s)$=0. For the DC bus voltage control, a simple PI controller is used in the outer-loop. The DC bus voltage control has a very slow dynamics relative to the higher frequency resonance interactions due to the current loop. Therefore, only the current control loop dynamics is taken into account while doing stability analysis. Fig. 4 shows the bode plots of the VSC input admittance $Y(s)$ and the equivalent admittance seen by the VSC, i.e., $1/Z_{eq}(s)$. The phase response of $Y(s)$ goes below -90^o around 1667Hz which matches with f_{crit} for $T_d = 1.5T_s$.

TABLE I. PARAMETERS: CASE 1

VSC parameters		
L_1	Converter side inductor	1.5mH
L_2	Grid side inductor	0.7mH
C	Filter capacitor	10μF
C_{dc}	DC bus capacitor	3mF
V_{dc}	DC bus voltage	200V
f_s	Switching frequency	10kHz
Grid parameters		
V_g	Grid voltage	120V
f_1	Grid frequency	60Hz
Z_g	Grid impedance	50μH
Current Control Parameters		
K_p	Proportional gain	5.7
$K_{R,1}$	Resonant gain at f_1	500
DC Bus Voltage Control Parameters		
K_{pd}	Proportional gain	3.7
K_{Id}	Integral gain	16.8

From the magnitude plots, it can be observed that the two magnitude response curves intersect twice with the second intersecting point around 2.35kHz lying in the non-passive region of the converter admittance. At this point, $Y(s)$ exhibits inductive behavior and $1/Z_{eq}(s)$ exhibits capacitive behavior which triggers LC resonance and the non-passive VSC admittance amplifies the resonance leading to instability.

By changing the LCL filter parameters, the single VSC mentioned here can be made stable, which is shown in *Case 2*.

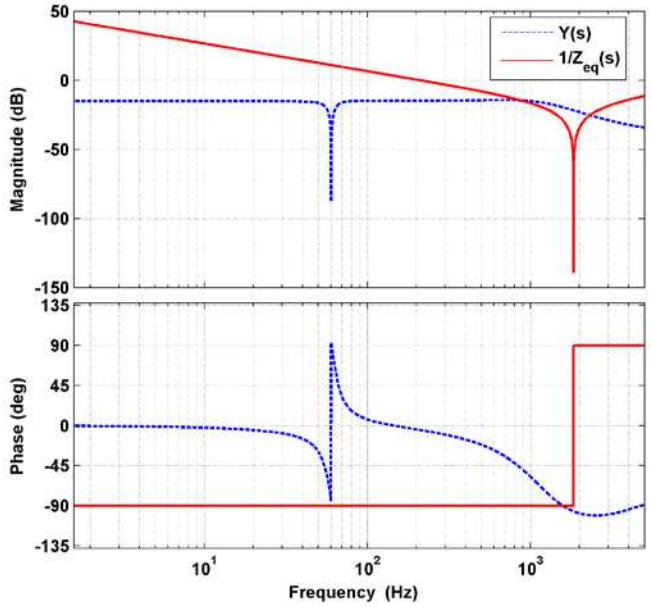

Fig. 4. Frequency response of VSC input admittance and equivalent grid admittance for *Case 1*.

B. *Case 2: Multiple VSC interaction*

All control parameters for *Case 2* are kept the same as in *Case 1*, as the converter side inductor is identical in both cases. With larger grid side inductor L_2, filter capacitor C or a larger grid inductance L_g, the resonant point may move into the passive admittance region which can stabilize the single VSC operation. One such scenario is shown in Table II. Even though the new set of parameters stabilize the single VSC current loop, addition of even an identical VSC unit to the POC may destabilize the system. Such destabilizing effect of multiple-converter interaction is investigated in *Case 2*. A capacitor C_g is added at the point of common coupling (POC) as shown in Fig. 5.

TABLE II. PARAMETERS: CASE 2

VSC parameters		
L_1	Converter side inductor	1.5mH
L_2	Grid side inductor	2mH
C	Filter capacitor	30μF
Grid parameters		
Z_g	Grid impedance	0.8mH
C_g	Capacitor placed at POC	22μF

Fig. 6 shows the frequency response of the equivalent admittance seen by the VSC with the new system parameters. With a single VSC, the intersecting point between $Y_1(s)$ and

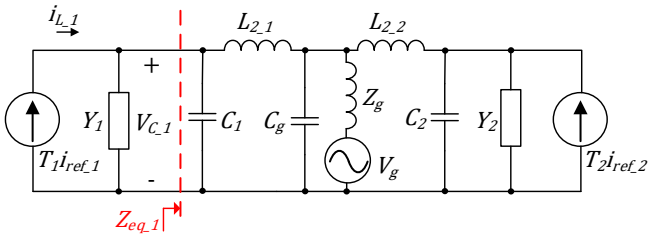

Fig. 5. Impedance model of the two-VSC system in *Case 2*.

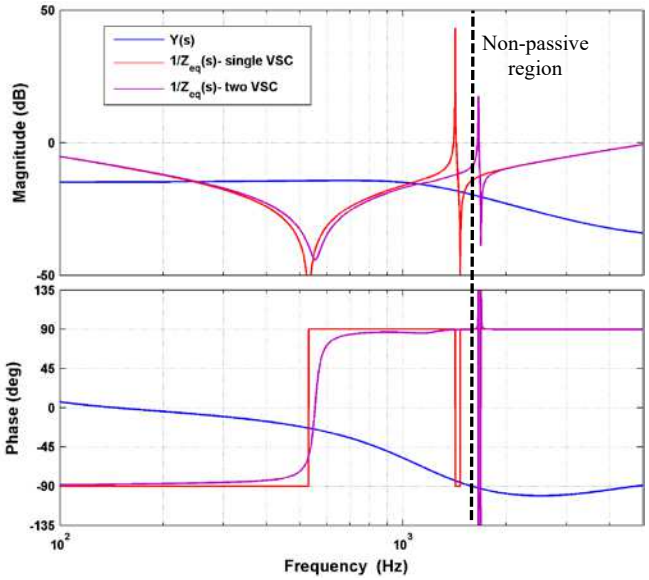

Fig. 6. Frequency response of VSC input admittance and equivalent grid admittance for single VSC and two-VSC system in *Case 2*.

$1/Z_{eq\_1}(s)$, i.e., the resonant point, lies within the passive region which results in stable operation. However, if another identical VSC is added at the POC, the resulting equivalent admittance moves the resonant point into the non-passive region, which causes the two-VSC system to become unstable.

V. Predictive Current Control

A predictive current controller (PCC) can be utilized to achieve passive converter admittance. Fig. 7 shows the sampling and PWM update instants for such a predictive control scheme.

From the values of inductor current i_L^{k-1}, DC bus voltage v_{dc}^{k-1} and voltage across LCL filter capacitor v_c^{k-1} sampled at $(k-1)$-th sampling instant and switching duty ratio d^{k-1}, the inductor current $i_L^{k,p}$ at end of k-th switching period is predicted. Comparing $i_L^{k,p}$ with inductor current reference i_{ref}^{k}, switching duty ratio for the next PWM period is calculated. Over one switching period, the DC bus voltage is assumed to be constant at $v_{dc}^{k,p} = v_{dc}^{k-1}$. Prediction of capacitor voltage can be obtained assuming that three samples are equally spaced or that it is constant over one switching period, i.e., $v_c^{k,p} = v_c^{k-1}$; the latter assumption is used here.

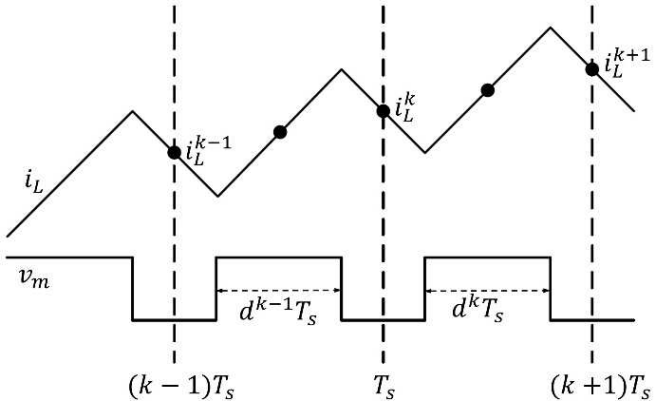

Fig. 7. Switching scheme for predictive current control.

L_e is a model parameter used by the controller as the value of the converter side inductor L_1.

$$i_L^{k,p} = i_L^{k-1} + \frac{T_s}{L_e}(v_m^{k-1} - v_c^{k-1}) \quad (9)$$

$$v_m^k = \frac{L_e}{T_s}\left(i_{ref}^k - i_L^{k,p}\right) + v_c^{k,p} \quad (10)$$

To develop the admittance model for PCC, a continuous time model is built as shown in Fig. 8. Continuous time equivalent of the controller is obtained using $Z^{-1} = e^{-sT_s}$. From the model, input admittance for PCC is derived as follows.

$$Y(s) = \frac{1-2F(s)}{sL_1 + FL_e/T_s} \quad (11)$$

where $$F(s) = \frac{e^{-sT_s}(1-e^{-sT_s})}{sT_s(1+e^{-sT_s})} \quad (12)$$

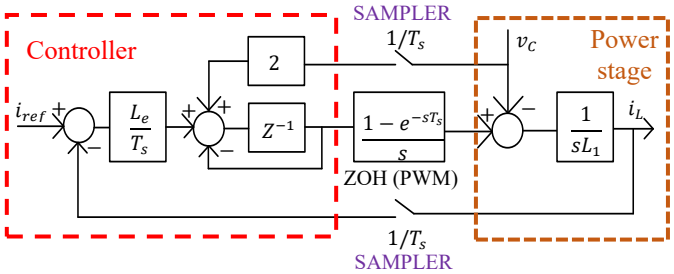

(a) Hybrid model of a VSC with predictive control.

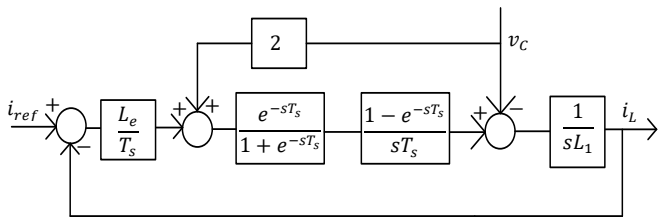

(b) Continuous time equivalent model.

Fig. 8. Derivation of continuous time model of a VSC with PCC. PWM process is approximated with a ZOH.

Fig. 9 shows the frequency response of $Y(s)$ and the equivalent admittance seen by the VSC for both *Case 1* and *Case 2*. In the experiment, to account for the drop in inductance value due to magnetic saturation, $L_e = 0.75$mH is used. From the phase response, it is evident that the predictive controller achieves passive admittance almost up to the Nyquist point, and therefore, achieves stable operation in both cases.

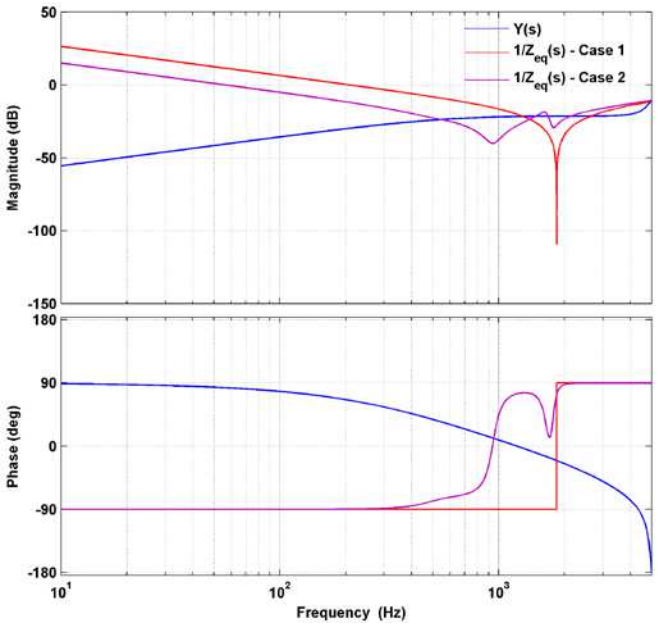

Fig. 9. Frequency response of VSC input admittance and equivalent grid admittance seen by VSCs for predictive current control.

VI. Simulation Results

To validate the frequency domain analysis, time domain simulations are done in MATLAB-Simulink with PLECS Blockset using nonlinear switching models of the converters. In Simulink, the implicit stiff solver ode23t is used to avoid divergence for marginally stable systems, and to better capture the high frequency oscillations.

A. Case 1

Fig. 10 shows the simulated waveforms for *Case 1*. Keeping the DC bus voltage control loop the same, performance of the proportional-resonant (PR) controller is compared with that of the predictive controller. At $t = 0.15s$, the inner loop is switched from predictive control to PR control. From the current waveshape, it is evident that the predictive controller achieves stable current control whereas the PR controller leads to harmonic resonance. Performing FFT on the current waveform, the resonance frequency is found to be at around 2.4kHz as shown in Fig. 11 which matches well with the prediction from the passivity based analysis.

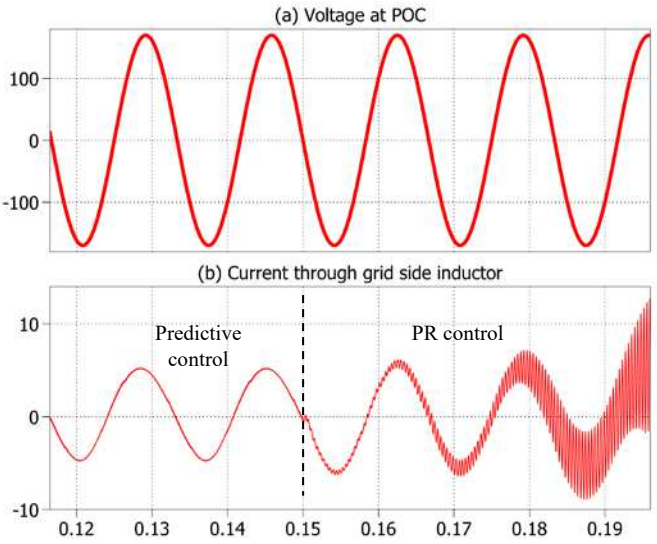

Fig. 10. *Case 1*: Grid-tied, single VSC operation: (a) Voltage at the point of common coupling; (b) current through the grid side inductor. At t=0.15s, the inner loop is switched from predictive current controller to PR controller.

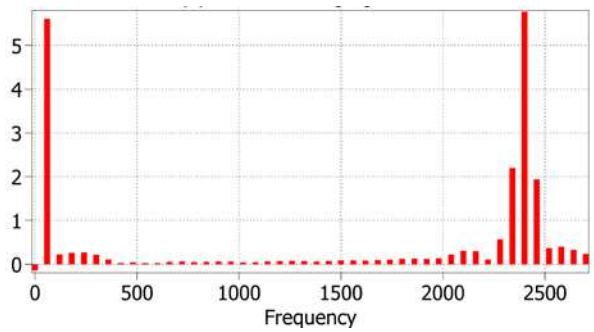

Fig. 11. FFT of output current with PR control for *Case 1*.

B. *Case 2*

Fig. 12(a) shows the output current shapes for the single converter operation before adding the second VSC with a PR controller in *Case 2*. The admittance plot predicted stable operation for this operating condition which matches with the simulated output. Now if two converters are connected to the grid, the network poles shift and overlap with the negative conductance region which results in an unstable system. The simulated waveforms for both VSCs exhibit oscillations of very high frequency and magnitude which is shown in Fig. 12(b). From FFTs of the current waveforms, the oscillations in both cases occur at around ≈1680Hz as shown in Fig. 13, which matches with the frequency domain analysis. Using the stabilizing predictive controller developed, stable output is obtained for the same two converter case in *Case 2* as shown in Fig. 12(c).

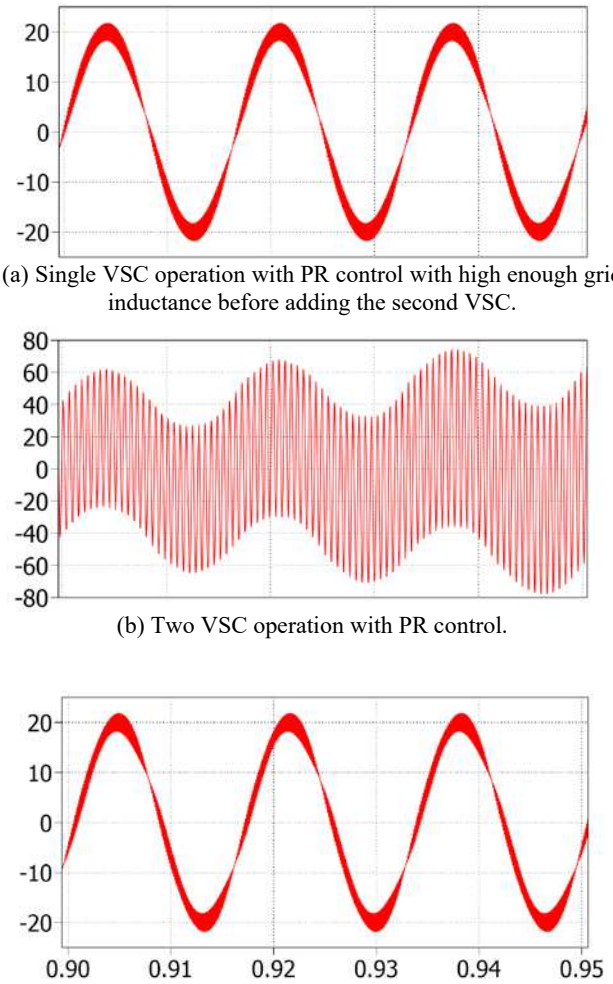

(a) Single VSC operation with PR control with high enough grid inductance before adding the second VSC.

(b) Two VSC operation with PR control.

(c) Two VSC operation with predictive current control.

Fig. 12. Simulated current through converter side inductor for *Case 2*.

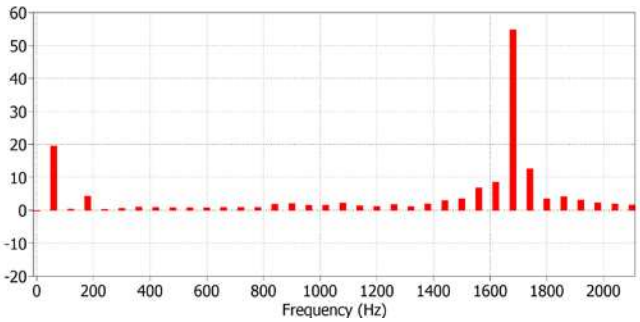

Fig. 13. FFT of output current with PR control for *Case 2*.

VII. Experimental Results

To validate the stabilizing property of the predictive current controller, experimental setup was made for *Case 1*. A high bandwidth AC source was used to emulate the grid and an

external inductor was used to emulate the grid impedance. Digital control was implemented using a TI 28377 single core floating-point digital signal processor. As the PR controller is not stable, the VSC went through the start-up sequence employing the predictive controller with the inductor model of $L_e = 0.5mH$. After establishing a stable DC bus voltage with unity-power-factor operation, the inner loop was switched to PR control using the parameters listed in Table I. Harmonic resonance is triggered by the PR controller and the experimental current shape matches very closely to the simulated waveform as shown in Fig. 14. Later in the experiment, the inner loop is switched back to predictive control but with a different model parameter of $L_e = 1mH$. For this implemented system, a dominant variation is observed in the inductor value due to magnetic saturation where the inductance drops as the current increases. In the experiment, powdered core, i.e., HighFlux core with μ=60, was used for the inductor. From no load to full load of 18A, the inductance varies approximately from 1.7mH to 0.9mH. The experimental result shows that with two different values of L_e for the predictive controller, satisfactory result is obtained.

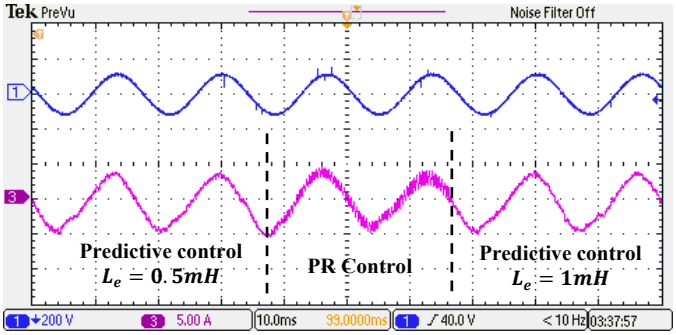

Fig. 14. Voltage measured at POC (blue) and current through the grid side inductor (pink). Predictive control achieves stable operation with two different model setting, i.e. $L_e = 0.5mH, 1mH$. PR control leads to harmonic resonance.

Existing active damping methods to stabilize harmonic resonance instabilities involve additional sensors or extensive optimization process or powerful processor for faster calculation, all of which are quite complicated from implementation standpoint. In contrast, the stabilizing predictive control dramatically simplifies the implementation and does not require any additional sensors since a voltage sensor is typically included for grid synchronization.

VIII. Conclusion

Predictive current control method has been adopted to prevent harmonic resonance instabilities in grid-tied VSCs interconnected in a power system. Using Laplace domain analysis, the admittance model for the predictive control of converter side current is derived which is shown to be passive up to frequencies very close to the Nyquist point. Predictive control is simple and very easy to implement compared to existing active damping methods for preventing such harmonic resonance instabilities in that frequency range. Performance of the controller was satisfactory irrespective of model imperfections. The frequency domain analysis was validated by simulations and hardware experiments both of which matched very closely to the frequency domain passivity based analysis.

Acknowledgement

This work is supported by the National Science Foundation under award number EEC-0812121 for the FREEDM Engineering Research Center.

References

[1] R. Beres, X. Wang, F. Blaabjerg, M. Liserre and C. Bak, "Optimal Design of High-Order Passive-Damped Filters for Grid-Connected Applications," *IEEE Transactions on Power Electronics*, vol. 31, no. 3, pp. 2083-2098, 2016.

[2] X. Wang, F. Blaabjerg and P. Loh, "High-performance feedback-type active damping of LCL-filtered voltage source converters," *2015 IEEE Energy Conversion Congress and Exposition (ECCE)*, 2015.

[3] L. Zhou, Y. Chen, A. Luo, J. Guerrero, X. Zhou, Z. Chen and W. Wu, "Robust two degrees-of-freedom single-current control strategy for LCL-type grid-connected DG system under grid-frequency fluctuation and grid-impedance variation," *IET Power Electronics*, vol. 9, no. 14, pp. 2682-2691, 2016.

[4] Q. Ye, R. Mo, Y. Shi and H. Li, "A unified Impedance-based Stability Criterion (UIBSC) for paralleled grid-tied inverters using global minor loop gain (GMLG)," *2015 IEEE Energy Conversion Congress and Exposition (ECCE)*, 2015.

[5] X. Wang, F. Blaabjerg, M. Liserre, Z. Chen, J. He and Y. Li, "An Active Damper for Stabilizing Power-Electronics-Based AC Systems," *IEEE Transactions on Power Electronics*, vol. 29, no. 7, pp. 3318-3329, 2014.

[6] D. Yang, X. Ruan and H. Wu, "A Real-Time Computation Method With Dual Sampling Mode to Improve the Current Control Performance of the *LCL*-Type Grid-Connected Inverter," *IEEE Transactions on Industrial Electronics*, vol. 62, no. 7, pp. 4563-4572, 2015.

[7] X. Wang, F. Blaabjerg and P. Loh, "Passivity-Based Stability Analysis and Damping Injection for Multi-Paralleled Voltage-Source Converters with LCL Filters," *IEEE Transactions on Power Electronics*, pp. 1-1, 2017.

[8] L. Harnefors, X. Wang, A. Yepes and F. Blaabjerg, "Passivity-Based Stability Assessment of Grid-Connected VSCs—An Overview," *IEEE Journal of Emerging and Selected Topics in Power Electronics*, vol. 4, no. 1, pp. 116-125, 2016.

[9] L. Harnefors, A. Yepes, A. Vidal and J. Doval-Gandoy, "Passivity-Based Controller Design of Grid-Connected VSCs for Prevention of Electrical Resonance Instability," *IEEE Transactions on Industrial Electronics*, vol. 62, no. 2, pp. 702-710, 2015.

[10] L. Harnefors, L. Zhang and M. Bongiorno, "Frequency-domain passivity-based current controller design," *IET Power Electronics*, vol. 1, no. 4, p. 455, 2008.

[11] J. Fischer, S. Gonzalez, M. Herran, M. Judewicz and D. Carrica, "Calculation-Delay Tolerant Predictive Current Controller for Three-Phase Inverters," *IEEE Transactions on Industrial Informatics*, vol. 10, no. 1, pp. 233-242, 2014.

[12] J. Castello, J. Espi and R. Garcia-Gil, "A New Generalized Robust Predictive Current Control for Grid-Connected Inverters Compensates Anti-Aliasing Filters Delay," *IEEE Transactions on Industrial Electronics*, vol. 63, no. 7, pp. 4485-4494, 2016.

[13] S. Lissandron, L. Dalla Santa, P. Mattavelli and B. Wen, "Experimental Validation for Impedance-Based Small-Signal Stability Analysis of Single-Phase Interconnected Power Systems With Grid-Feeding Inverters," *IEEE Journal of Emerging and Selected Topics in Power Electronics*, vol. 4, no. 1, pp. 103-115, 2016.

[14] S. Buso and P. Mattavelli, *Digital Control in Power Electronics*. San Rafael, CA, USA: Morgan & Claypool, 2006.

[15] Y. Tang, W. Yao, P. Loh and F. Blaabjerg, "Design of LCL Filters With LCL Resonance Frequencies Beyond the Nyquist Frequency for Grid-Connected Converters," *IEEE Journal of Emerging and Selected Topics in Power Electronics*, vol. 4, no. 1, pp. 3-14, 2016.

[16] L. Harnefors, R. Finger, X. Wang, H. Bai and F. Blaabjerg, "VSC Input-Admittance Modeling and Analysis Above the Nyquist Frequency for Passivity-Based Stability Assessment," *IEEE Transactions on Industrial Electronics*, pp. 1-1, 2017.

[17] Z. Song and D. Sarwate, "The frequency spectrum of pulse width modulated signals," *Signal Processing*, vol. 83, no. 10, pp. 2227-2258, 2003.